Journal of Power Sources 247 (2014) 618–628

Contents lists available at ScienceDirect

Journal of Power Sources

journal homepage: www.elsevier.com/locate/jpowsour

Temperature-dependent electrochemical heat generation in a commercial lithium-ion battery

Todd M. Bandhauer [a], Srinivas Garimella [b,*], Thomas F. Fuller [c]

[a] Interdisciplinary Thermal Science Laboratory, Department of Mechanical Engineering, Colorado State University, Fort Collins, CO 80525, USA
[b] Sustainable Thermal Systems Laboratory, GWW School of Mechanical Engineering, Georgia Institute of Technology, Love Building, Room 340, 801 Ferst Drive, Atlanta, GA 30382, USA
[c] Center for Innovative Fuel Cell and Battery Technologies, Georgia Tech Research Institute and School of Chemical & Biomolecular Engineering, Georgia Institute of Technology, Atlanta, GA 30332, USA

HIGHLIGHTS

- Measured temperature-dependent electrochemical heat generation on C/$LiFePO_4$ cell.
- Total heat generation is a strong function of current, temperature, and DoD.
- Entropic heating significant up to 5*C* and in a charge depletion dynamic profile.
- Galvanostatic data predicts dynamic performance well.

ARTICLE INFO

Article history:
Received 28 May 2013
Received in revised form
29 July 2013
Accepted 1 August 2013
Available online 14 August 2013

Keywords:
Battery
Lithium-ion
Heat generation
Temperature-dependent

ABSTRACT

Lithium-ion batteries suffer from inherent thermal limitations (i.e., capacity fade and thermal runaway); thus, it is critical to understand heat generation experienced in the batteries under normal operation. In the current study, reversible and irreversible electrochemical heat generation rates were measured experimentally on a small commercially available C/$LiFePO_4$ lithium-ion battery designed for high-rate applications. The battery was tested over a wide range of temperatures (10–60 °C) and discharge and charge rates (~*C*/4–5*C*) to elucidate their effects. Two samples were tested in a specially designed wind tunnel to maintain constant battery surface temperature within a maximum variation of ±0.88 °C. A data normalization technique was employed to account for the observed capacity fade, which was largest at the highest rates. The heat rate was shown to increase with both increasing rate and decreasing temperature, and the reversible heat rate was shown to be significant even at the highest rate and temperature (7.4% at 5*C* and 55 °C). Results from cycling the battery using a dynamic power profile also showed that constant-current data predict the dynamic performance data well. In addition, the reversible heat rate in the dynamic simulation was shown to be significant, especially for charge-depleting HEV applications.

1. Introduction

Lithium-ion batteries have been targeted for use in electric and hybrid electric vehicles (EV and HEV) due to their high energy and power densities compared to those of other secondary battery chemistries. However, these batteries have not realized widespread commercialization in large format applications, and suffer from inherent thermal limitations [1]. At temperatures above ~90 °C, various exothermic reactions are triggered, potentially leading to thermal runaway [2,3]. In addition, these batteries generally lose capacity and power capability rapidly when repeatedly cycled or soaked at cell temperatures greater than ~50 °C (e.g., Refs. [4–7]). Therefore, it is desirable to maintain a lower battery temperature (~25 °C) during cell operation. This cell temperature is determined from the balance of heat generation and storage, and heat removal by the associated thermal management system. Thus, understanding of the heat generation characteristics in lithium-ion batteries is essential for maintaining safety and improving cycle lifetime.

2. Battery heat generation

The local electrochemical heat generation rate can be been calculated using the following equation:

* Corresponding author. Tel.: +1 404 894 7479; fax: +1 404 894 1658.
E-mail address: sgarimella@gatech.edu (S. Garimella).

0378-7753/$ – see front matter © 2013 Elsevier B.V. All rights reserved.
http://dx.doi.org/10.1016/j.jpowsour.2013.08.015

$$q''' = \frac{i}{\text{vol}}\left(U - V - T\frac{\partial U}{\partial T}\right) \quad (1)$$

This equation has frequently been cited in the literature and associated with the study of Bernardi et al. [8], although it was used much earlier (e.g., Sherfey and Brenner [9]). The irreversible overpotential ($\eta_{irr} = U - V$) is due to ohmic losses in the cell, charge-transfer resistance at the interface, and mass transfer limitations. The entropic overpotential ($\eta_{rev} = -T\partial U/\partial T$) arises from the electrochemical reaction, and the derivative of the open-circuit potential with respect to temperature is often referred to as the entropic heat coefficient. This heat rate is considered reversible because the magnitude is the same and only the sign is different for charging and discharging at the same rate. This equation may be readily applied to estimate the amount of electrochemical heat generation in lithium-ion batteries if there is no heat of mixing, no phase change other than crystalline phase transitions, no spatial variation in temperature or state of charge (SoC), only one electrochemical reaction occurring at each electrode, and negligible joule heating in the current collectors. In lithium-ion batteries without side reactions, there is only one reaction occurring at each electrode, and no phase-change effects other than crystalline phase transitions exist. Neglecting the heat of mixing terms is acceptable for low discharge rates and for high discharge rates when the particle size is sufficiently small, which is representative of commercial battery designs [10].

There have been multiple attempts to experimentally determine the irreversible electrochemical heat generation rate for lithium-ion batteries. The primary experimental methods are accelerated-rate calorimetry (ARC) [11–13] and isothermal heat conduction calorimetry (IHC) [14–27]. The ARC method consists of measuring the heat rejected by the battery during operation while encapsulated in either air or a solid material (e.g., Styrofoam). In this method, the temperature of the battery is allowed to rise as heat is transferred through the medium to a constant temperature sink. The heat generation rate is estimated using an energy balance between the battery and the heat sink. For IHC, the battery remains at one temperature throughout operation using an isothermal well in close contact with the surface of the battery (e.g., liquid or a metal heat sink). High-accuracy thermopiles either embedded inside the heat sink or placed near the surface of the battery are used to measure the heat rate. As in all calorimetric methods, considerable data manipulation or special experimental procedures are usually required due to the phase lag resulting from long instrument time constants (i.e., time elapsed from heat generation to measurement).

The reversible heat has been estimated using a variety of techniques. Several methods are used to estimate the entropic heat coefficient (i.e., $\partial U/\partial T$). The most common method is to measure the open-circuit potential (OCP) variation with temperature at a fixed SoC [11–14,19,20,22,26–28]. The other methods are calorimeter based. Several authors have assumed that irreversible heat remained constant upon charge and discharge. Hence, they subtracted the charge calorimeter data from the discharge data, which cancels the overpotential heat, and allows for the entropic heat to be determined as follows:

$$q_{ent} = \frac{q_{dis} - q_{cha}}{2} \quad (2)$$

Thomas et al. [29] showed that this method provided results similar to those from their SoC cycling method. Onda et al. [22] also showed that this method produced results similar to those of the direct measurement of OCP vs. temperature. However, Hong et al. [13] observed that this method produced entropic heat coefficients that were a function of rate, which may be attributable to inaccuracies in their measurement technique. Another calorimetric method is to subtract an estimated irreversible heat from the total heat. The overpotential heat is typically (and most accurately) estimated by direct calculation using OCP and operating voltage data [18–21].

A detailed discussion of the results gleaned from the relevant techniques for measuring total and reversible heat generation rate is provided elsewhere [1]. However, a few aspects relevant to this study are discussed here. First, there are relatively few investigations [11,25,26] that measure total heat generation for currents greater than 1*C*, and none for currents higher than 2*C*. In addition, the majority of the studies has been conducted at one temperature (near nominal ambient: 20–25 °C), and few studies have investigated the impact of temperature on heat generation. For those that have investigated temperature influences, the range of temperatures is typically small. The studies of Saito et al. [23] and Kobayashi et al. [16] have the largest temperature ranges (20–60 °C and 25–60 °C, respectively), but they only tested batteries discharged at low current (*C*/10). Thomas and Newman [10] and Hong et al. [13] tested higher rates, but with a more narrow temperature range (15–30 °C and 35–55 °C, respectively). In both of these studies, no appreciable difference in heat generation was observed for the temperatures tested. Moreover, the measured overall heat generation for these batteries is not large (at most a peak of 84.5 W L^{-1} for the 0.92*C* rate at the end of discharge [22]). Small temperature changes inside the battery can lead to significant heat accumulation, which, in some cases, can be larger than the heat rejected by the device [13]. Accurate measurement of the battery temperature and heat capacity is therefore required for these techniques. In addition, as the rate increases, maintaining constant temperature may not be achievable with the IHC method, which was implied by Lu and Prakash [20].

The effective overpotential due to entropic heating appears to be of the same order of magnitude as the actual overpotential at the moderately high 1*C* rate. This has also been shown in a recently published review paper to be true across a variety of different cell chemistries [30]. In addition, some studies show that the heat rate profile has a highly non-linear S-shaped curve even at the 1*C* rate, which can be attributed to entropic heating (e.g., Bang et al. [14] and Kim et al. [15]). Thus, it is clear that the entropic heat should not be neglected or overly simplified by using a constant or a linear curve fit for battery thermal simulations.

3. Present investigation

HEV applications require high rates of charge and discharge over a wide range of environmental conditions. In addition, little information has been published on the heat generation effects observed in the C/$LiFePO_4$ lithium-ion battery system, which is currently being targeted for the HEV and EV markets. Thus, in the current investigation, the open-circuit potential and operation overpotential are measured on a commercially available C/$LiFePO_4$ lithium-ion battery designed for high-rate applications. Where appropriate, performance variation between two samples is discussed. These data are used to estimate the magnitudes of irreversible and reversible heats over a wide range of charge and discharge rates (up to 5*C*) and temperatures (10–60 °C). This method has been shown previously to be accurate for estimating the heat generation rate for small cells when heat of mixing is negligible [26]. Details of the experimental techniques, procedures, and uncertainties are provided first, followed by discussions of the procedure necessary to account for observed capacity fade. Thereafter, the relative magnitudes of each heat effect are presented and discussed in detail. Finally, data collected on a battery sample tested using an HEV simulation power profile are

presented, and are then compared to heat generation rate and performance data gathered for galvanostatic discharge and charge.

4. Commercial battery description

Two samples of an 18650 battery commercially available from K2 Energy Systems (model LFP18650P) were tested in this investigation. The battery contains a carbonaceous negative electrode and $LiFePO_4$ positive electrode, separated by a porous separator (most likely polypropylene or a similar polymer). The electrolyte consists of 10% by weight of $LiPF_6$ salt and 30/30/30% by weight EC/DMC/EC aqueous solvent. A sample battery was cut open to accurately determine the thickness of the composite electrodes (including current collectors) and separator (Table 1). The sample unit cell for this battery consists of negative and positive composite electrodes and two porous separators. The composite electrodes are metal current collectors (copper for the negative and aluminum for the positive) coated on both sides with the porous electrode material. Thus, the unit cell thickness is 0.284 mm. Using the width of the "jelly roll" (58.74 mm) and length of the smallest (positive) electrode (782.6 mm), the approximate heat generation volume is 13.08 mL. The estimated heat rates are divided by this volume to obtain the local volumetric heat generation rate. The published capacity for this battery is 1.25 Ah, and, as described below, two samples were tested.

5. Experimental setup

5.1. Reversible heat generation

The reversible heat generation is calculated using the entropic heat coefficient, which, in this investigation, is determined from the slope of OCP vs. temperature at a specified SoC for both samples. Cell potential was measured using an Arbin BT-2000 battery cycling unit (4 channels, −25 A to 25 A and 0–10 VDC per channel) with a calibrated uncertainty discussed below. Two cells were tested simultaneously, and two Type K surface mount temperature probes (Omega part SA1-K-72-SC) were affixed to each battery to the battery surface during operation using electrical tape. The fixture was placed in a programmable environmental chamber (Associated Environmental Systems model BHD-508) to ensure constant battery temperature over a wide range.

The following testing procedure was used. To ensure that the battery begins at the same SoC for all tests, the battery was first charged at a constant rate of 0.5 A to a voltage of 3.65 V. Thereafter, the battery was held at 3.65 V and taper-charged to 50 mA. This procedure was conducted at a 30 °C battery temperature to eliminate the influence of temperature on charging. At this stage, the battery depth of discharge (DoD) is assumed to be 0 Ah. After charging, the battery was discharged at 50 mA for 3 h to a DoD of 0.15 Ah while maintaining a 30 °C battery temperature. The battery was then allowed to rest for 4 h at 30 °C. Thereafter, the environmental chamber temperature was decreased to 10 °C and held for 2 h. The subsequent soak temperatures increased in 10 °C increments up to 60 °C, with each held for 2 h. Data points were collected at each soak temperature beginning at 10 °C once every minute. After the soak at 60 °C, the soak temperature was decreased to 30 °C, and held for 1 h. Thereafter, the battery was discharged in 0.05 Ah increments at 50 mA up to a DoD of 0.95 Ah. For all tests, the slope of the last 20 data points (i.e., 20 min) was never greater than 0.031 °C min^{-1} or 0.066 mV min^{-1} for the average test temperature and potential, respectively. As discussed below, the entropic heat coefficient at each SoC is determined from the linear slope calculated using the method of least squares over the entire temperature range.

Table 1
Summary of commercial battery unit cell thicknesses.

Component	Thickness [mm]
Cu current collector	0.036
Electrode material (1-side)	0.033
Composite negative electrode	*0.102*
Al current collector	0.036
Electrode material (1-side)	0.048
Composite positive electrode	*0.132*
Separator (1 sheet)	*0.025*
Total unit cell	*0.284*

5.2. Irreversible heat generation

As mentioned above, the irreversible heat generation rate is calculated from the cell overpotential. The OCP was determined first for the two sample batteries using the method described above, while the method for estimating the operation potential is described here. When the charge and discharge rates increase, the volumetric heat generation rate increases. Thus, the low surface convection inside the environmental chamber causes the battery temperature to rise more rapidly as the rate increases. Therefore, a specially designed wind tunnel with built-in temperature control (Fig. 1) was fabricated to ensure a constant surface temperature throughout all operation potential tests. In this test facility, a centrifugal blower (AMETEK Nautilair 8.9″ model 150330-00) forces air through a heat exchanger coupled to a primary coolant loop. This controls the temperature of the air flowing over the battery, which is placed in a rectangular ductwork (41 mm × 79 mm × 305 mm) downstream of the heat exchanger. A mixing fan is placed between the heat exchanger and the battery ductwork to ensure uniform air temperature over the battery. The temperature of the primary coolant is controlled using a secondary heat exchanger (not shown) that is coupled to a colder secondary coolant (i.e., building chilled water) and a 1 kW immersion heater for fine control. The secondary coolant can also be directly supplied to the primary coolant loop if colder temperatures than achievable through the secondary heat exchanger are desired. Throughout each test, adjustments were made to the heater power and coolant flow rates to maintain a constant battery surface temperature. (It should be noted that it is the battery surface temperature, not the internal temperature, that is maintained constant in this manner – an isothermal interior is not possible to achieve without internal cooling of the batteries.) The battery surface temperature is the arithmetic average of 4 thermocouples placed on the surface of the battery.

During operation, the battery was held at a constant current using the same battery cycler used in the OCP tests. Sample 1 was tested for both charge and discharge over a DoD range from 0.15 Ah to 0.95 Ah at rates of 0.25 A, 0.5 A, 1 A, 2 A, 3 A, and 5 A. The test procedure for both samples is described here. As in the method used for OCP, the battery was first charged at 0.5 A to 3.65 V, followed by a taper charge to 50 mA while maintaining a 25 °C surface temperature. Upon charging, the battery was immediately discharged at 1 A to a DoD of 0.15 Ah. At this stage, adjustments were made to heater power and coolant flow rates to achieve the desired battery surface temperature. The maximum time elapsed during this adjustment was 30 min. The battery was then discharged at the testing rate to a DoD of 0.95 Ah, followed by a 10 min rest period. At high discharge rates, it was not possible to discharge to 0.95 Ah. If this occurs, the battery was discharged to a DoD of 0.95 Ah at a rate of 0.5 A so that all charge tests began at the same DoD. After resting, charging at the same rate commences until either a DoD of 0.15 Ah, or an operation voltage of 4.2 V was reached.

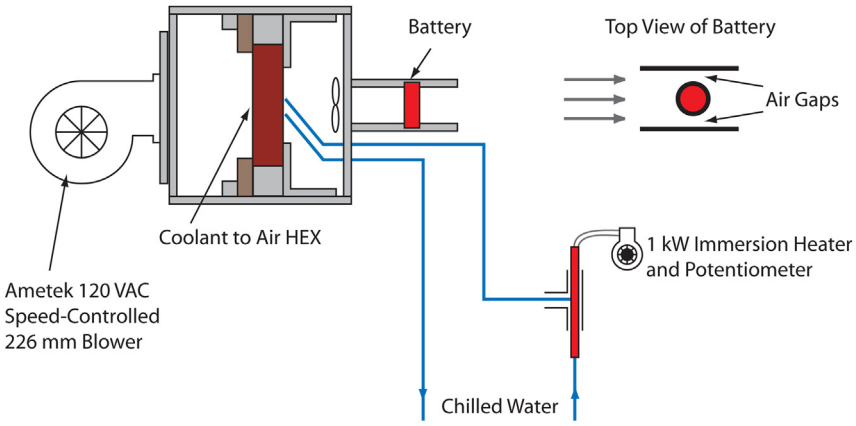

Fig. 1. Temperature-controlled wind tunnel used for battery operation tests.

To document and account for capacity fade and sample variability, the tests on battery Sample 1 were conducted in single current batches. A test batch consisted of five separate tests at the same current, but at different temperatures, ranging from 15 °C to 55 °C in 10 °C increments. After each test batch (including the OCP tests), a reference performance test was also conducted to document capacity degradation during the tests (Fig. 2). The batteries in these reference tests were charged according to the same regimen, followed by a 10 min rest and subsequent discharge to 2.5 V at 1 A. Sample 2 was tested primarily to document sample variation, and it was also used in a dynamic profile test (discussed below) at three temperatures: 15 °C, 35 °C, and 55 °C. The following discharge and charge rates and temperatures were tested on Sample 2: 0.5 A and 3.0 A at 25 °C, and 1.0 A at 15 °C and 55 °C. Three reference tests were conducted: after the OCP, repeatability, and dynamic tests.

Estimation of uncertainties in the measurements and results is shown in detail in Appendix A. Table 2 summarizes the bias and precision uncertainties for the measured voltage, temperature, and current, assuming a 95% confidence interval. Using the procedure documented in Appendix A, the entropic heat coefficients are known to within $\pm 9.93\ \mu V\ K^{-1}$ and $\pm 13.43\ \mu V\ K^{-1}$ for Samples 1 and 2, respectively. Using the maximum total uncertainties in temperature, current, overpotential, and entropic heat coefficient, the maximum uncertainty for the total volumetric heat generation rate for Sample 1 varied from $\pm 0.06\ W\ L^{-1}$ at 0.25 A to $\pm 2.84\ W\ L^{-1}$ at 3 A.

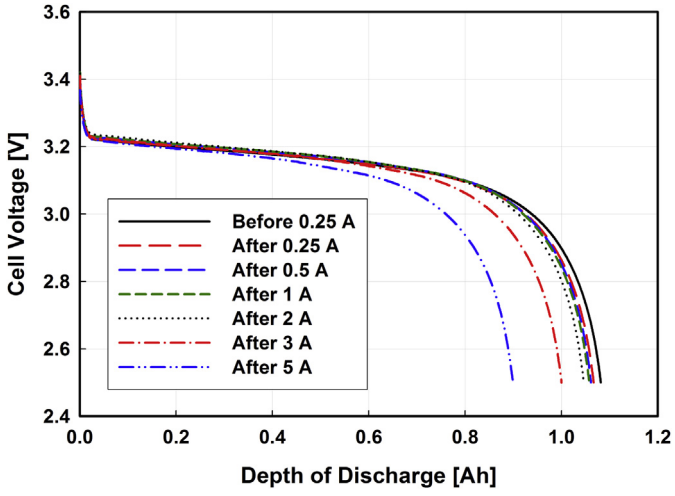

Fig. 2. Reference performance tests for Sample 1.

6. Results and discussion

The experimental results are presented and discussed here. First a data normalization procedure that accounts for the observed capacity fade is discussed. Variation in OCP, operation potential, and entropic heat coefficient between the two samples are then shown to be minimal. Thereafter, to understand the relative importance of the two electrochemical heat modes, the relative magnitudes of the irreversible and reversible electrochemical overpotentials during charge and discharge are presented. The total estimated volumetric heat generation rate is then presented, followed by a discussion of performance characteristics and predicted heat generation using a power profile generated from the US06 High Speed Drive Cycle [31].

6.1. Data normalization

As stated previously, the sample batteries lose capacity as repeated testing proceeds, especially at increased rates and temperatures. Fig. 2 shows the operation voltage vs. discharged capacity for the six reference capacity tests conducted on Sample 1. As can be seen in this figure, the capacity dropped precipitously as

Table 2
Maximum precision and bias uncertainties for measured quantities.

Item	Detail	Value
Precision - OCP tests		
Voltage		0.035 mV
Temperature		0.016 °C
Precision – Operation tests		
Voltage		0.729 mV
Temperature		1.29 °C
Current		1.71 mA
Bias		
Voltage	Channel 1	0.427 mV
	Channel 2	0.559 mV
Temperature	Thermocouple 1	0.156 °C
	Thermocouple 2	[a]
	Thermocouple 3	0.170 °C
	Thermocouple 4	0.167 °C
Current	0.25 A and 0.5 A	2 mA
	1–5 A	50 mA

[a] Assumed equal to thermocouple 1.

testing progressed, especially after the battery was tested at 3 A and 5 A. If the overpotential is calculated using the same discharge capacity location for the operation and OCP tests, significant errors may result, especially near a DoD of 0.95 Ah. Thus, all data collected are normalized using the estimated battery capacity at the 1*C* discharge rate (Norm_{Cap}), which is calculated from averaging the reference test rate (1 A) and the discharge capacities before and after the tests conducted at each rate batch ($\text{Before}_{\text{Cap}}$ and $\text{After}_{\text{Cap}}$, respectively) as follows:

$$\text{Norm}_{\text{Cap}} = \frac{2 \times 1[\text{Ah}] + \text{Before}_{\text{Cap}} + \text{After}_{\text{Cap}}}{4} \tag{3}$$

Instead of iterating on the discharge rate, it was assumed that the normalized cell capacity was the arithmetic average of the measured capacity and the assumed 1 Ah capacity utilized for each test. Table 3 shows Norm_{Cap} for each test rate and the OCP tests for Sample 1. The discharge capacity in Ah is divided by the estimated Norm_{Cap} to obtain the normalized DoD. (It should be noted that the first reference test was conducted after the OCP tests. Therefore, it was assumed that the capacity fade was minimal, and, thus, the discharge capacity at the 1*C* rate determined from the first reference test sufficiently normalized the data.) Fig. 3 shows that the voltage curves for the reference tests nearly collapse onto the same curve when plotted vs. normalized DoD. However, the voltage curve for the 5 A test appears to be slightly lower than those for all other tests. For example, at a normalized DoD of 0.8, the operation potential is 53.4 mV lower for the 5 A test than for the 0.25 A test. In either case, these results appear consistent with the study by Liu et al. [5], which shows that the capacity is controlled by the amount of cyclable lithium. Lithium is consumed when the negative electrode solid-electrolyte interphase is damaged and subsequently repaired, which may explain the increase in resistance seen after the 5 A tests.

6.2. Sample variation

Two samples were tested to observe variations due to processing and manufacturing. Fig. 4 shows a comparison of the results for the two samples under the following conditions: OCP at 30 °C, 0.5 A, 1.0 A, and 3.0 A at 25 °C, 1.0 A at 15 °C, and 1.0 A at 55 °C. When normalized, the results show remarkably little variation between samples for these test conditions. The largest operation potential deviation appears at the end of discharge at the highest compared rate (3.0 A), with Sample 1 operating at 0.15 V below Sample 2. This results in a volumetric heat rate difference of 34.4 W L^{-1}, which is significant. However, this difference is most probably due to a larger capacity fade for Sample 1, which was cycled much more than Sample 2. In addition, the 1 A tests were conducted before the 3 A tests for Sample 1, and, thus, the increased number of cycles over a wider range of temperatures also contributed to the larger observed battery aging for this sample at the higher rate.

Table 3
Estimated battery capacities for each test batch on Sample 1.

Preceding tests	Capacity [Ah]
OCP	1.041
0.25 A	1.034
0.5 A	1.031
1.0 A	1.029
2.0 A	1.023
3.0 A	1.000
5.0 A	0.950

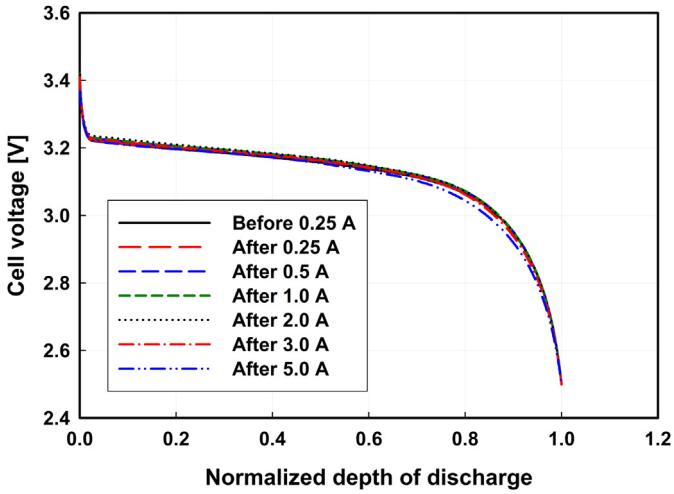

Fig. 3. Normalized reference performance tests for Sample 1.

6.3. Entropic heat coefficient

The dependence of OCP on temperature is shown in Fig. 5 for Sample 1. This relationship appears to be linear over most of the range of DoD considered here, which has also been shown for other chemistries (e.g., Hong et al. [13] and Thomas et al. [29]). The entropic heat coefficient and correlation coefficient (R^2) for Samples 1 and 2 are plotted as a function of normalized DoD in Fig. 6. The entropic heat coefficient at a given DoD is determined from the slope of OCP vs. temperature graph using the method of least squares for a linear curve fit as follows:

$$\frac{\partial U}{\partial T} = \frac{\sum_{i=1}^{N} (T_i - \overline{T})(U_i - \overline{U})}{\sum_{i=1}^{N} (T_i - \overline{T})^2} \tag{4}$$

When the state of charge is near zero or one, the correlation coefficients deviate significantly from unity, suggesting that the relationship is not linear. However, the non-linearity is most likely due to the uncertainty in measured voltage (maximum of 0.428 mV for Sample 1). For example, at the lowest normalized DoD for Sample 1, the difference in OCP between 10 °C and 60 °C is only 1.29 mV. Conversely, at a normalized DoD of 0.532, the difference in OCP between the same two temperatures is 9.91 mV. Thus, better accuracy on the measured voltage is required to improve the accuracy of the entropic heat coefficient when it is near zero. As shown in Fig. 6, there is little variation in both the magnitude and trend of entropic heat coefficient over the tested normalized DoD between the two samples.

6.4. Irreversible and reversible overpotential

Representative irreversible and reversible overpotentials measured for Sample 1 are shown in Fig. 7 for discharge and charge. The overpotentials are calculated as follows:

$$\eta_{\text{irr}} = U - V \tag{5}$$

$$\eta_{\text{rev}} = -T\frac{\partial U}{\partial T} \tag{6}$$

Thus, the irreversible overpotential will always be positive for discharge, but negative for charge. The reversible overpotential is independent of charge and discharge. The value of the reversible

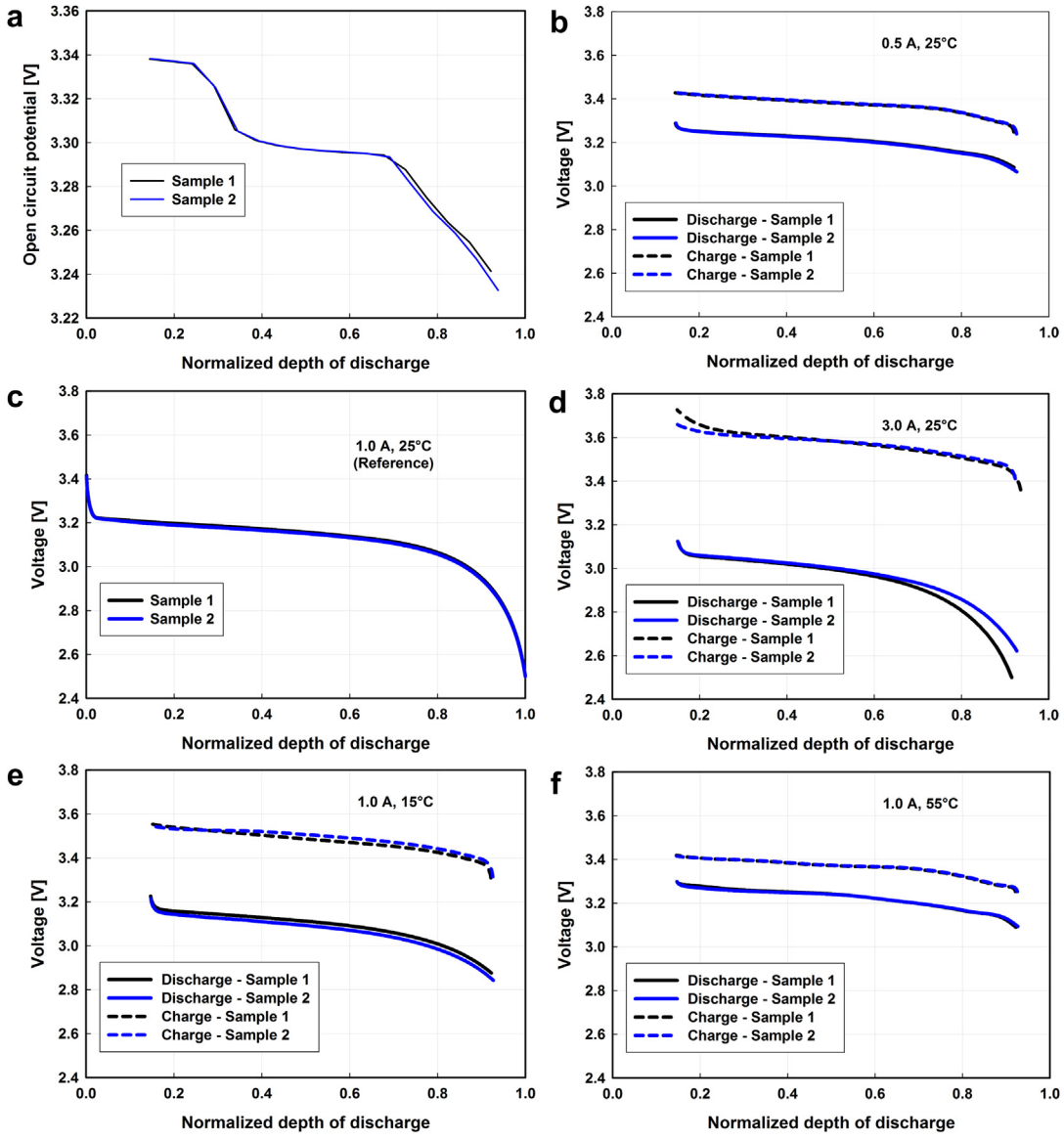

Fig. 4. Comparison between Samples 1 and 2: (a) OCP at 30 °C, (b) 0.5 A at 25 °C, (c) 1.0 A at 25 °C, (d) 3.0 A at 25 °C, (e) 1.0 A at 15 °C, and (f) 1.0 A at 55 °C.

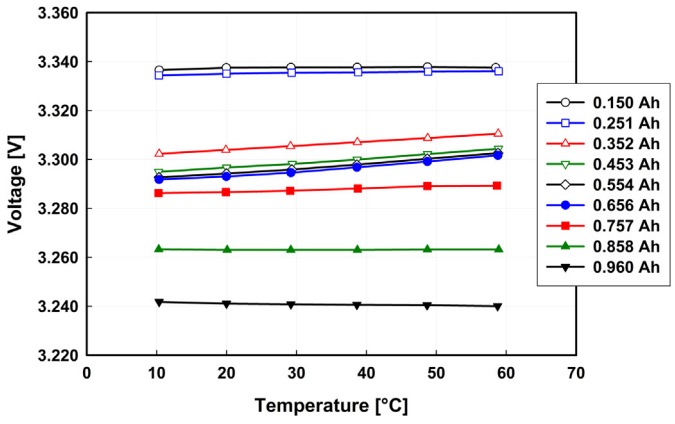

Fig. 5. OCP vs. temperature for Sample 1.

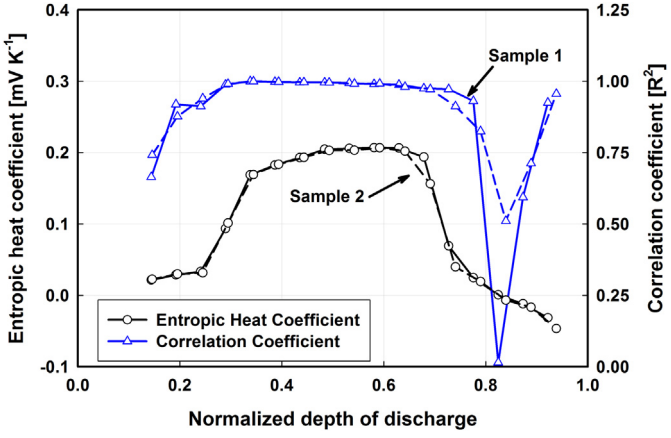

Fig. 6. Entropic heat coefficient and correlation coefficient for Samples 1 and 2.

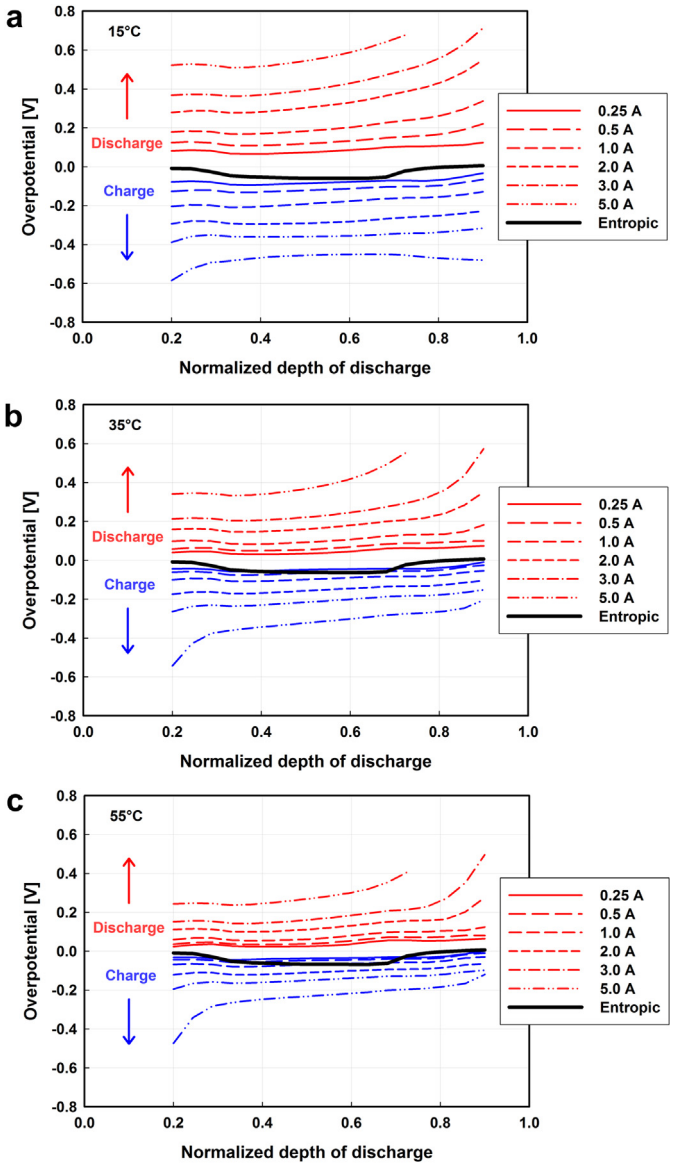

Fig. 7. Reversible and irreversible discharge and charge overpotentials for Sample 1: (a) 15 °C, (b) 35 °C, and (c) 55 °C.

overpotential is primarily negative for the DoD range in this investigation because the entropic heat coefficient is mostly positive (see Fig. 6). As expected, the irreversible overpotential is a strong function of rate. For example, at a normalized DoD of 0.506 and a test temperature of 35 °C, the irreversible overpotential increases from 0.034 V to 0.369 V when the discharge rate increases from 0.25 A to 5 A. Similarly, the overpotential decreases from −0.048 V to −0.322 V over the same rates when charging. However, the change in irreversible overpotential with rate depends strongly on the temperature. For example, at the same normalized DoD and rates, the discharge irreversible overpotential increases from 0.074 V to 0.546 V at 15 °C, but only from 0.026 V to 0.270 V at 55 °C. Similarly, the overpotential decreases from −0.085 V to −0.456 V at 15 °C and from −0.036 V to −0.231 V at 55 °C at the same conditions. This suggests that the electrochemical heat generation rate is a strong function of temperature between 15 °C and 55 °C, especially for high rates. This is not surprising, because it has been shown that both transport properties and kinetics are functions of temperature in lithium-ion batteries [32,33]. The irreversible overpotential is also a function of normalized DoD. There appears to be a large overpotential increase and decrease near the end of discharge and charge, respectively. This is because the electrochemical reactions can no longer be sustained due to the depletion of lithium in the negative and positive electrodes, respectively. This effect is more pronounced, primarily as the rate increases, and secondarily as the temperature increases. For example, at 3 A and 55 °C, the overpotential ranges from 0.142 V to 0.227 V when discharged from 0.200 to 0.769 normalized DoD, but it increases to 0.496 V at a normalized DoD = 0.900. Conversely, at 35 °C, the irreversible overpotential at the same rate increases from 0.204 V to 0.318 V when discharged from a normalized DoD of 0.200 to 0.769 and ends at 0.573 V at 0.900. Furthermore, the overpotential range for 0.5 A at 15 °C over the entire discharge range is only 0.107–0.220 V. This effect is even more pronounced for charging, where exothermic reversible heat augmented the irreversible heat between normalized DoDs of 0.35 and 0.7. As a result, the rapid increase in charge overpotential near the end of charging appears to be primarily a function of rate. For example, when charged at 5 A, the irreversible overpotential at a normalized DoD of 0.2 (i.e., near the end of charge) ranged from only −0.585 V to −0.474 V between test temperatures of 15 °C and 55 °C, respectively. However, between the normalized DoDs of 0.288 and 0.900, the overpotential at this same rate ranged from −0.450 to −0.493 and from −0.120 to −0.283 for these same temperatures, respectively.

Although the reversible overpotential is not a strong function of temperature, the reversible overpotential appears to be significant, even at the highest rates. This can be seen easily in the charge overpotential curves because the reversible and irreversible contributions are both negative. However, as the temperature decreases, the irreversible overpotential increases significantly due to mass transport and kinetic limitations, while there is little change in the reversible overpotential. Thus, the relative contribution of the reversible heat to the total electrochemical heat decreases as the temperature decreases. For example, at 55 °C, the ratio of reversible to irreversible overpotential is 0.292 at a 5 A charge rate and a normalized DoD of 0.506. In contrast, this ratio decreases to 0.197 and 0.130 at 35 °C and 15 °C, respectively. For discharge at the same rate, this ratio changes from −0.109 to −0.250 as the temperature increases from 15 °C to 55 °C. The impact of reversible heat on the total heat evolved is not clear for a battery that is being rapidly cycled in an HEV application due to the changing relative impacts as both the DoD and rate change. Nevertheless, it is clear that reversible heating will be significant. This is discussed below.

6.5. Total volumetric heat generation rate

Using the overpotential results with the applied current and estimated unit cell volume (13.08 mL), the total volumetric heat generation rate is calculated using Equation (1). The current is positive and negative for discharging and charging, respectively. Representative high-rate results at 35 °C for Sample 1 are shown in Fig. 8. The magnitudes of total volumetric heat generation rate appear to be consistent with previously measured values on different chemistries. For example, at 35 °C and a discharge rate of 1 A (which is nominally the 1*C* rate), the total volumetric heat rate ranges from 1.98 W L^{-1} to 14.4 W L^{-1} between a normalized DoD of 0.2 and 0.9. By comparison, the volumetric heat generation rate ranged from 0 W L^{-1} to 27.7 W L^{-1} at the same test temperature for a variety of lithium-ion batteries tested by Al Hallaj et al. [11] with different carbon-based negative electrodes and a $LiCoO_2$ positive electrode [1].

When compared to the irreversible overpotentials, the total volumetric heat rate appears to be strongly influenced by the

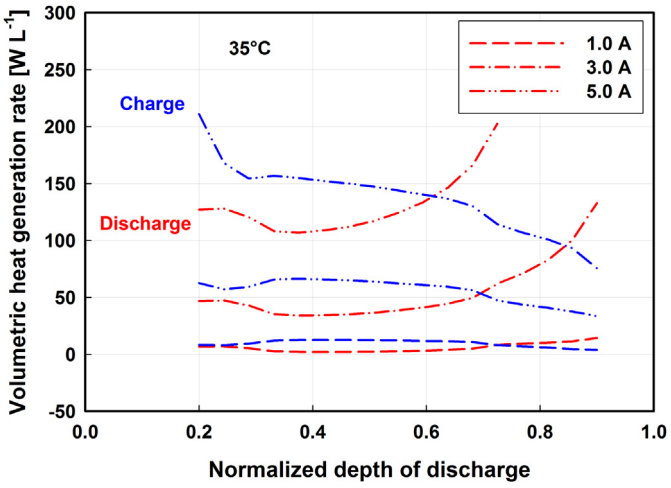

Fig. 8. Total discharge and charge volumetric heating rate for Sample 1 at 35 °C.

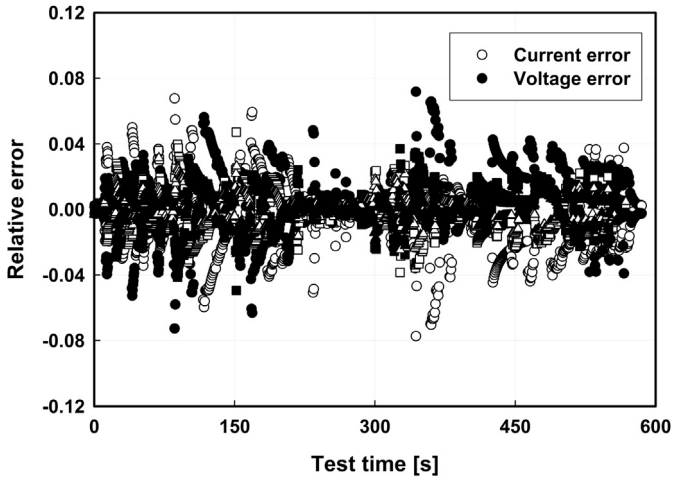

Fig. 10. Relative error of current and voltage for the dynamic simulation predicted from constant-current data.

reversible heat rate. For example, there is a significant reduction in the total discharge heating rate over the normalized DoD range of 0.35–0.7 where the entropic heat coefficient is at its maximum values (Fig. 6). Similarly, charge heating is increased over the same range. As a result, there is a larger rise in total heat rate for discharge and a smaller rise for charge than would be expected if only the irreversible overpotential were considered. This can be clearly seen in the total heat generation rate at 3 A and 35 °C. Over the normalized DoD range from 0.2 to 0.9, the heat generation rate varies between 34.0 and 132.8 W L^{-1} when discharged, but only from 33.5 W L^{-1} to 62.5 W L^{-1} when charged. To further understand the impact of reversible heating on the total volumetric heat, Fig. 9 shows the absolute value of the ratio of total reversible to total irreversible heat energy generated for discharge and charge, respectively. The ratio increases as the temperature increases for all rates. As the temperature increases, the cell overpotential decreases, while the reversible heat remains approximately the same over the tested test range. In addition, the overpotential increases with rate, which causes the ratio to decrease. It is clear that the irreversible heat dominates in all but a few cases, especially at the higher rates and lower temperatures. However, reversible heat is not a negligible quantity, even being 7.5% of the total heat when discharged at 15 °C and 5 A. This significant influence of reversible heating may be attributable to the cell design, which was intended for high-rate applications. The total electrode material thickness (162 μm) was only 57% of the total unit cell thickness (284 μm, Table 1). In other cell designs intended for higher energy density, the total electrode thickness may be a higher percentage, which significantly increases the mass transport resistance and may dominate any temperature related effects. However, because this is the first study to adequately control battery temperature during measurement, additional research on alternative battery designs is needed.

6.6. US06 drive cycle

After the above tests were complete, Sample 2 (the less cycled battery) was subjected to the US06 drive cycle, which represents aggressive highway driving. The battery power requirements for an HEV application were generated using Powertrain System Analysis Toolkit (PSAT) for Georgia Tech's EcoCAR student led team competition [34]. A 2012 Saturn Vue parallel/series hybrid was redesigned with a 1.6 L engine and a 9.6 kWh battery pack coupled to a planetary gear set. For the present investigation, it was assumed that 3000 individual batteries (39.23 L) were required to replace the existing battery pack. The battery was placed in the same wind tunnel as for the operation voltage tests, where the surface temperature was controlled at three different test temperatures: 15 °C, 35 °C, and 55 °C. The battery was cycled beginning at a normalized

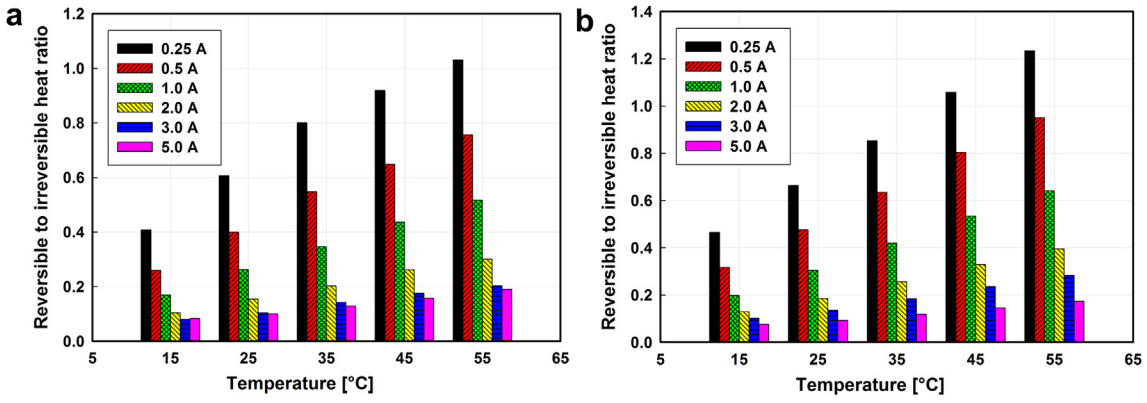

Fig. 9. Ratio of cumulative reversible heat to irreversible heat for (a) discharge, and (b) charge.

Table 4
Summary of dynamic simulations tests: ending DoD and cumulative heat generation.

Test temperature [°C]	DoD at EoD [Ah]		Total heat dissipation [J]	
	Predicted	Actual	Predicted	Actual
15	0.552	0.550	193.4	166.9
35	0.543	0.541	96.63	72.07
55	0.543	0.541	61.63	44.8

DoD of 0.48. The constant power required from and delivered to the battery was controlled using the same Arbin BT-2000 battery controller used previously.

This experiment was conducted to answer the following questions:

- Can constant-current data reasonably predict the performance of a dynamic power profile?
- Is it better to use constant-current or dynamic profile data to predict the heat generation rate in an HEV application?
- What are the effects of reversible heating during an HEV simulation?

In the following discussion, predicted values refer to predictions based on the previously collected constant-current data (using linear interpolation), whereas measured refers to the data collected during the dynamic simulation.

Fig. 10 shows the relative error between predicted and measured values, defined as follows:

$$\text{Relative Error} = \frac{\text{Predicted} - \text{Measured}}{\text{Measured}} \tag{7}$$

As can be seen in Fig. 10, the current and voltage are both predicted within ±8% of the measured value, with 90% of the data predicted within ±2.5%. As a result, the charge depletion rate in the cycled battery is nearly the same for each method (see Table 4). However, in the dynamic simulation, sometimes the switching between charge and discharge is so rapid that the overpotential has a sign opposite of what is expected. For example, at 35 °C between 326.1 s and 326.6 s, the battery switches from being discharged at 2.77 W to being charged at 1.14 W. Fig. 11 shows that although the battery is being charged, it has a positive overpotential, which suggests an unrealistic negative irreversible heat. In this and similar cases, the

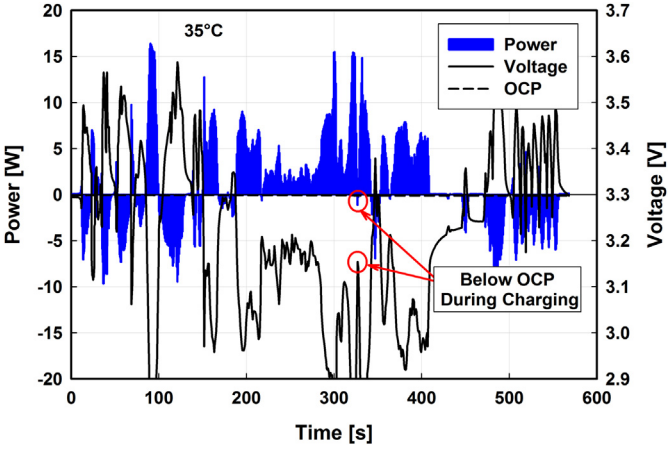

Fig. 11. Performance during dynamic discharge cycle at 55 °C.

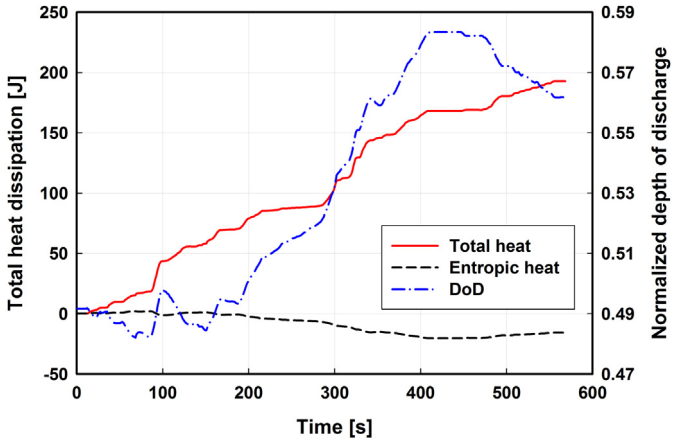

Fig. 12. Cumulative reversible and total heat and DoD for dynamic simulation at 15 °C.

predicted data always yield positive values for irreversible heating. Furthermore, the dynamic test here is a charge-depleting cycle, and, as a result, the cumulative heat predicted is larger than estimated directly from the measurements (see Table 4). How accurately the heat generation rate is predicted from constant-current data for a dynamic cycle remains an open question, but it is clear from the results that one cannot directly use the dynamic data.

The effect of entropic heating is observed in Fig. 12 for the 15 °C test, which has the lowest reversible heat contribution due to increased overpotential at this low temperature. It has been suggested by Smith and Wang [35] that during HEV applications, reversible heating can be neglected. The cumulative impact from reversible heat should generally be negligible if the battery is cycled about a fixed SoC, and if the charge and discharge rates are nominally the same. As shown in Fig. 12, when the battery was cycled back to its original SoC at 118 s and 160 s, the cumulative reversible heat was indeed negligible. However, as the battery was depleted, it becomes significant. For example, at 15 °C, the total heat load was reduced by 7.5% when reversible heat is included.

7. Conclusions and recommendations

Entropic heat coefficient and reversible heat rate for a commercially available C/$LiFePO_4$ lithium-ion battery were determined using OCP vs. temperature data ranging from 10 °C to 60 °C. Irreversible heat generation rates were estimated on a commercially available cell for both discharge and charge at rates up to 5 A for temperatures ranging from 15 °C to 55 °C. During the irreversible tests, the battery surface temperature was maintained constant by using a specially designed wind tunnel that allows for rapid adjustment to the time-varying heat generation rate, which kept it within ±0.88 °C for all tests. Data normalization was required to account for capacity fade, which is significant and appears to occur more rapidly at higher rates. After normalization, the reference tests conducted at periodic intervals collapsed onto the same discharge curve, and little variation was observed between two different samples. The total electrochemical heat generation rate was found to be a strong function of rate and temperature between 15 °C and 55 °C. The total heat generation rate was significantly affected by reversible heat, even at rates as high as 5 A. The reversible heat contribution is largest at higher temperatures and lower rates, which tend to reduce the irreversible overpotential.

A dynamic cycle profile based on the US06 drive cycle showed that reasonably good prediction of actual data can be achieved using constant-current data (which were on a different sample).

Thus, the constant-current data can be used to estimate cell performance in a dynamic simulation for this particular battery design. However, this conclusion should be verified for other battery designs, especially those with thicker electrodes and/or higher operation overpotentials. For this battery design and particular HEV simulation, the cumulative reversible heating appears negligible when the battery returns to the original SoC, but significant when charge depleting. In other applications, this may not be true. Thus it is important to include accurate reversible heating estimations during battery thermal simulations. Furthermore, the results from this investigation show that battery thermal models must account for temperature-dependent heat and current generation when assessing the impact of thermal management in large battery packs. The complexity of these thermal models can potentially be reduced by utilizing temperature-dependent, constant-current data, which can enable investigation even when the battery is subjected to a dynamic load.

Acknowledgments

The authors gratefully acknowledge Sandia National Laboratories for providing a Graduate Research Fellowship for Dr. Bandhauer through the Excellence in Engineering Graduate Research Program. The authors also acknowledge the ARCS Foundation for providing additional funding to Dr. Bandhauer through the ARCS Scholars program.

Appendix A. Estimation of uncertainties

Uncertainties in the measurements and the results reported in this study are estimated using the approach described in Coleman and Steele [36]. Precision error, i.e., the random error about a measured quantity, can be estimated from statistical analysis of a sample data set assuming a t-distribution with $N-1$ degrees of freedom. The maximum precision uncertainties for the average voltage and temperature measured during the OCP tests are 0.035 mV and 0.016 °C, respectively. The maximum precision errors for average temperature and current measurements in the operation voltage tests are 1.29 °C and 1.71 mA, respectively. The operation voltage changes with time, thus it is conservatively assumed that the precision error is the same as the maximum precision error reported for the average voltage measurements, but for the next measured value instead of the next measured mean value. This results in an estimated precision error of 0.729 mV for the instantaneous voltage.

Bias error, i.e., the systematic error between the mean measured value and the true value, does not have an equivalent error that can be estimated from a sample data set. Furthermore, calibration does not remove all sources of uncertainty because measurement error can be inherent in both the calibration standard and measurement system. For example, the calibration curve fit may not perfectly predict the actual measured data, and thus is estimated as the standard error of estimate (SEE) as follows:

$$\mathrm{SEE}^2 = \frac{\sum_{i=1}^{N}\left[Y_i-(aX_i+b)\right]^2}{N-2} \tag{8}$$

The bias uncertainties assumed for this investigation are associated with the calibration standard and the SEE. Voltage measurements are calibrated using an Agilent 34401A digital multimeter, which has an uncertainty of 0.0035% of the measured value plus 0.0005% of full scale. The maximum measured value is 4.2 V and the voltage scale is 0–10 V. Thus, the maximum bias error associated with the calibration standard is 0.197 mV, which is conservatively assumed for all average voltage data collected on channels 1 and 2. The SEE for channels 1 and 2 are 0.379 mV and 0.523 mV, respectively. The total bias uncertainty (for a 95% confidence interval) is calculated as follows:

$$B_{\overline{V}} = \sqrt{B_{\mathrm{cs}}^2+4\mathrm{SEE}_{\overline{V}}^2} \tag{9}$$

Hence, the total bias uncertainties for the average voltage measured in the entropic heating tests are 0.427 mV and 0.559 mV for Samples 1 and 2, respectively. The bias error for the instantaneous voltage measurement on both samples is assumed to be the same as for Sample 1 (0.427 mV).

Similarly, for the average temperature, the bias errors arise from the calibration standard (±0.012 °C, Hart Scientific Model 1502A with platinum RTD probe) and the error from the calibration curve fit. For measurement calibration, the thermocouples were placed in a temperature-controlled bath (Hart Scientific Model 7340) in close proximity to the tip of the calibration standard RTD to eliminate bias from bath temperature non-uniformity. The total bias errors for thermocouples 1, 3 and 4 are 0.156 °C, 0.170 °C, and 0.167 °C, respectively. (Thermocouple 2 was damaged before calibration, and was assumed to have the same bias uncertainty as thermocouple 1.)

Because it is controlled during the tests, current was not calibrated. Thus, the bias error is assumed to be the published accuracy of the instrument: 0.1% of full scale. Two different scales were used during the test: −1 A to 1 A, and −25 A to 25 A. Therefore, for test currents of 0.25 A and 0.5 A, the bias error is 2 mA, while the bias errors for test currents 1–3 A, and 5 A are 50 mA.

The propagations of bias and precision uncertainties for a function f of many variables X_i are calculated as follows:

$$B_{f(X_i)}^2 = \sum_{i=1}^{J}\left[\left(B_{X_i}\frac{\partial f}{\partial X_i}\right)^2+\sum_{k=1}^{J}\frac{\partial f}{\partial X_i}\,\frac{\partial f}{\partial X_k}\rho_{ik}B_i'B_k'(1-\delta_{ik})\right] \tag{10}$$

$$P_{f(X_i)} = \left[\sum_{i=1}^{J}\left(P_{X_i}\frac{\partial f}{\partial X_i}\right)^2\right]^{1/2} \tag{11}$$

The additional term in the bias uncertainty propagation represents cross-correlation of measurement. It is assumed here that the correlation coefficient (ρ) between all temperature measurements and between all voltage measurements is equal to 1, where the Kronecker delta function is given by

$$\delta_{ik} = \begin{cases} 1 & i = k \\ 0 & i \neq k \end{cases} \tag{12}$$

Finally, the total uncertainty for a given quantity X_i is given by the following equation:

$$\mathrm{TU}^2 = B^2+P^2 \tag{13}$$

This equation holds for both measured and calculated quantities.

Nomenclature

a	curve fit slope
$\mathrm{After}_{\mathrm{Cap}}$	battery capacity after testing [Ah]
b	curve fit intercept
B	bias uncertainty
B'	correlated bias error
$\mathrm{Before}_{\mathrm{Cap}}$	battery capacity before testing [Ah]
DoD	depth of discharge [Ah]
$\partial U/\partial T$	entropic heat coefficient [V K^{-1}]

EoD	end of discharge
f	calculated function from measured values
i	current [A]
Measured	measured value during power performance test
N	number of samples
Norm_{Cap}	normalizing battery capacity [Ah]
P	precision uncertainty
Predicted	predicted value using constant-current data
q	total heat generation [J]
q'''	volumetric heat generation rate [W L^{-1}]
R^2	correlation coefficient
SEE	standard error of estimate
T	temperature [°C or K]
$\overline{T}$	average temperature [°C or K]
TU	total uncertainty
U	open-circuit potential [V]
$\overline{U}$	average open-circuit potential [V]
V	operation cell potential [V]
vol	unit cell volume [L]
X	measured value
Y	calculated value

Symbols

δ_{ik}	Kronecker delta function
ϕ	local potential in stack [V]
η	overpotential [V]
ρ_{ik}	cross-correlation coefficient

Subscripts

cha	charge
cs	calibration standard
dis	discharge
ent	entropic
i	summation index
irr	irreversible
j	summation index
rev	reversible
$\overline{V}$	average voltage

References

[1] T.M. Bandhauer, S. Garimella, T.F. Fuller, J. Electrochem. Soc. 158 (2011) R1.
[2] R. Spotnitz, J. Franklin, J. Power Sourc. 113 (2003) 81.
[3] H. Yang, S. Amiruddin, H.J. Bang, Y.K. Sun, J. Prakash, J. Ind. Eng. Chem. 12 (2006) 12.
[4] K. Amine, J. Liu, I. Belharouak, Electrochem. Commun. 7 (2005) 669.
[5] P. Liu, J. Wang, J. Hicks-Garner, E. Sherman, S. Soukiazian, M. Verbrugge, H. Tataria, J. Musser, P. Finamore, J. Electrochem. Soc. 157 (2010) A499.
[6] P. Ramadass, B. Haran, R. White, B.N. Popov, J. Power Sourc. 112 (2002) 606.
[7] P. Ramadass, B. Haran, R. White, B.N. Popov, J. Power Sourc. 112 (2002) 614.
[8] D. Bernardi, E. Pawlikowski, J. Newman, J. Electrochem. Soc. 132 (1985) 5.
[9] J.M. Sherfey, A. Brenner, J. Electrochem. Soc. 105 (1958) 665.
[10] K.E. Thomas, J. Newman, J. Electrochem. Soc. 150 (2003) A176.
[11] S. Al Hallaj, J. Prakash, J.R. Selman, J. Power Sourc. 87 (2000) 186.
[12] S. Al Hallaj, R. Venkatachalapathy, J. Prakash, J.R. Selman, J. Electrochem. Soc. 147 (2000) 2432.
[13] J.S. Hong, H. Maleki, S.A. Hallaj, L. Redey, J.R. Selman, J. Electrochem. Soc. 145 (1998) 1489.
[14] H. Bang, H. Yang, Y.K. Sun, J. Prakash, J. Electrochem. Soc. 152 (2005) A421.
[15] J.-S. Kim, J. Prakash, J.R. Selman, Electrochem. Solid State Lett. 4 (2001) A141.
[16] Y. Kobayashi, N. Kihira, K. Takei, H. Miyashiro, K. Kumai, N. Terada, R. Ishikawa, J. Power Sourc. 81–82 (1999) 463.
[17] Y. Kobayashi, H. Miyashiro, K. Kumai, K. Takei, T. Iwahori, I. Uchida, J. Electrochem. Soc. 149 (2002) A978.
[18] W. Lu, I. Belharouak, S.H. Park, Y.K. Sun, K. Amine, Electrochim. Acta 52 (2007) 5837.
[19] W. Lu, I. Belharouak, D. Vissers, K. Amine, J. Electrochem. Soc. 153 (2006) A2147.
[20] W. Lu, J. Prakash, J. Electrochem. Soc. 150 (2003) A262.
[21] W. Lu, H. Yang, J. Prakash, Electrochim. Acta 51 (2006) 1322.
[22] K. Onda, H. Kameyama, T. Hanamoto, K. Ito, J. Electrochem. Soc. 150 (2003) A285.
[23] Y. Saito, K. Kanari, K. Takano, J. Power Sourc. 68 (1997) 451.
[24] Y. Saito, K. Takano, K. Kanari, A. Negishi, K. Nozaki, K. Kato, J. Power Sourc. 97–98 (2001) 688.
[25] L. Song, J.W. Evans, J. Electrochem. Soc. 147 (2000) 2086.
[26] K.E. Thomas, J. Newman, J. Power Sourc. 119–121 (2003) 844.
[27] H. Yang, J. Prakash, J. Electrochem. Soc. 151 (2004) A1222.
[28] K. Onda, T. Ohshima, M. Nakayama, K. Fukuda, T. Araki, J. Power Sourc. 158 (2006) 535.
[29] K.E. Thomas, C. Bogatu, J. Newman, J. Electrochem. Soc. 148 (2001) A570.
[30] V.V. Viswanathan, D. Choi, D. Wang, W. Xu, S. Towne, R.E. Williford, J.-G. Zhang, J. Liu, Z. Yang, J. Power Sourc. 195 (2010) 3720.
[31] USEPA, 1996.
[32] K. Kumaresan, G. Sikha, R.E. White, J. Electrochem. Soc. 155 (2008) A164.
[33] L.O. Valoen, J.N. Reimers, J. Electrochem. Soc. 152 (2005) A882.
[34] R. Melsert, personal communication, 2009.
[35] K. Smith, C.Y. Wang, J. Power Sourc. 160 (2006) 662.
[36] H.W. Coleman, W.G. Steele, Experimentation and uncertainty analysis for engineers, Wiley, New York, 1989.